



Computational Analysis of the External Aerodynamics of the Unpowered X-57 Mod-III Aircraft

Presented at 2019 AIAA AVIATION, June 21th 2019

Seung Y. Yoo

NASA Armstrong Flight
Research Center

Jared C. Duensing

NASA Ames Research Center



Acknowledgement

- NASA Armstrong Team
 - Mike Frederick, Nicholas Johnson, Trong Bui, Thomas Matthews
- NASA Ames Team
 - Daniel Maldonado, Jeffrey A. Housman, James C. Jensen, Cetin C. Kiris
- NASA Langley Team
 - Karen A. Deere, Jeffrey K. Viken, Melissa B. Carter, Sally A. Viken



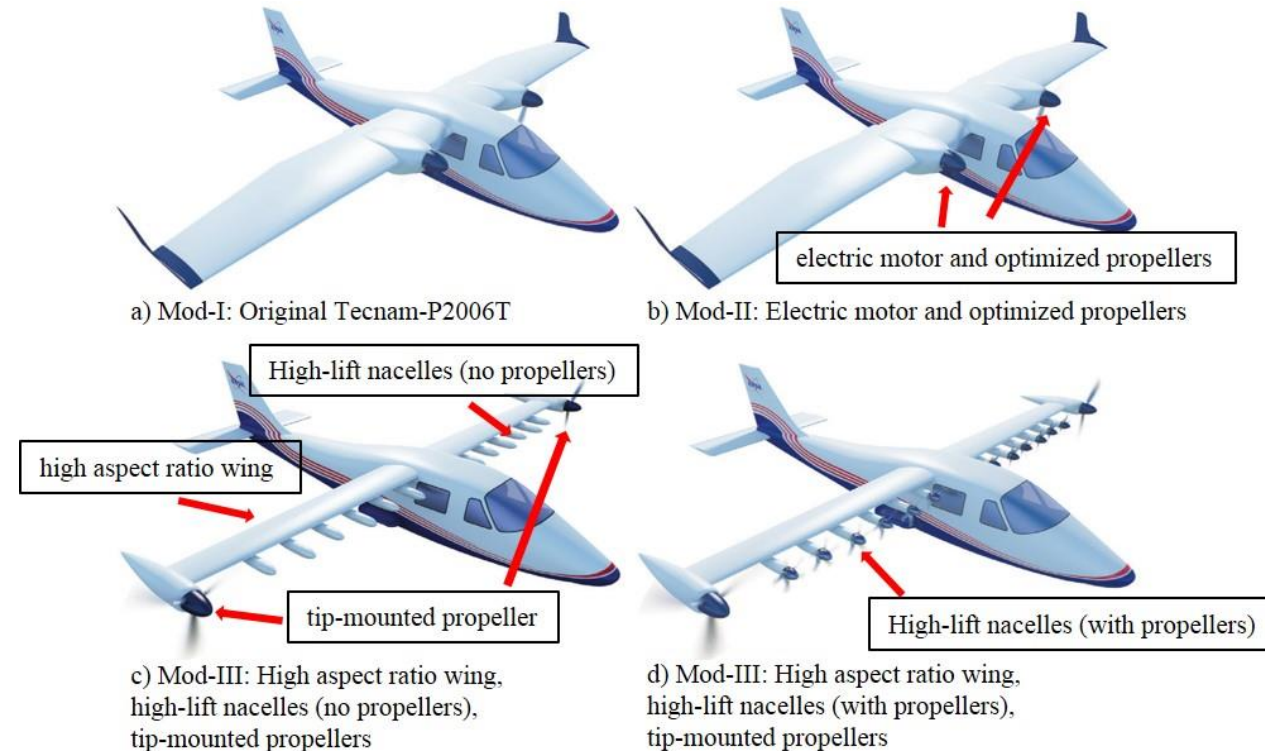
Outline

- Introduction
- Method
- Results
- Conclusion
- Questions



Introduction

- X-57 Program
 - Separated into multiple phases, denoted as “MOD”, to demonstrate various technologies
 - Electrical power-plant
 - Optimized high aspect ratio wing and high lift nacelle
 - Tip cruise motor for reducing induced drag
- Study focused on unpowered MOD-III
 - flow physics
 - differences in flow solution between CFD solvers
- Purpose of the study
 - Aerodynamic database generation for pilot-in-the-loop simulation
 - Understanding of the aerodynamics of the vehicle for flight safety
 - Baseline performance for powered simulation





Method

- STAR-CCM+ (v13.04.10)

- Used extensively at NASA AFRC for airworthiness analysis
- Grid
 - Unstructured polyhedral mesh
 - Half-span with symmetry boundary condition for symmetric flow, full-span for asymmetric flow simulation
- Solver
 - Steady state RANS
 - 2nd order Roe flux differencing scheme with algebraic multigrid solver with Gauss-Siedel relaxation scheme
 - Fully turbulent assumption, Spalart-Allmaras with rotational correction

- Launch Ascent Vehicle Analysis Framework

- Versatile NASA ARC developed framework consisting of multiple solvers
- Grid
 - Overset, structured, curvilinear grids
 - Full-span for all simulations
- Solver
 - Steady state RANS structured curvilinear solver
 - Second-order convective flux with Koren limiter
 - Fully turbulent flow assumption, Spalart-Allmaras turbulence rotational correction and quadratic constitutive relationship



Result

- Grid Refinement Study
- Angle of attack sweep
- Sideslip angle sweep



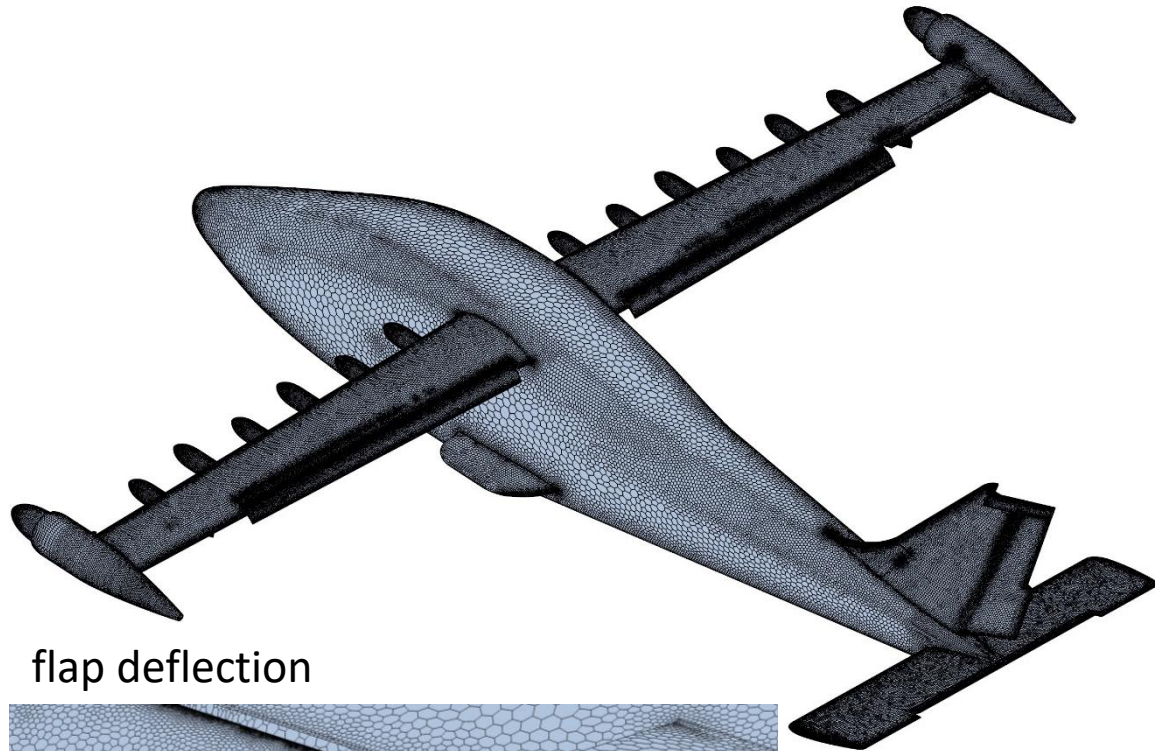
Result – Grid Refinement Study

- Atmospheric Condition
 - Altitude 2500 ft, Mach 0.139, freestream velocity = 153.87 ft/s
 - density $2.2078\text{E-}3\text{kg/m}^3$, static pressure = 1931.9 lbf/ft², static temperature 283.2K
 - Reynolds number $9.21\text{E}5$
 - Angle of attack = 10° , Sideslip angle = 20°
- Aircraft configuration
 - Aileron = -25°
 - Flap = 30°
 - Rudder = -28°
 - Stabilator = -15°
 - Pitch trim tab = -18°

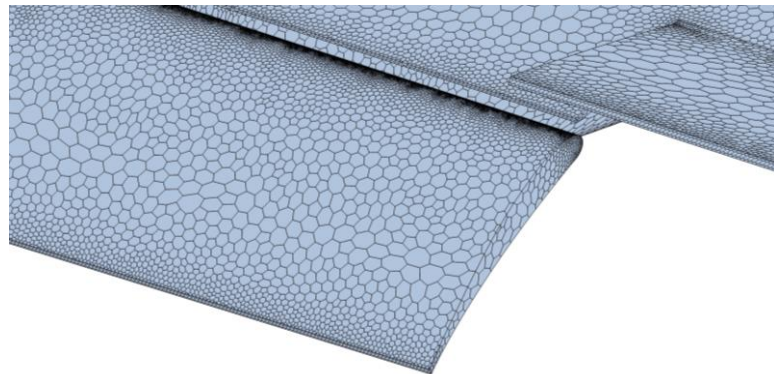


Result – Grid Refinement Study

- STAR-CCM+ Polyhedral Grid (coarse grid shown for clarity)



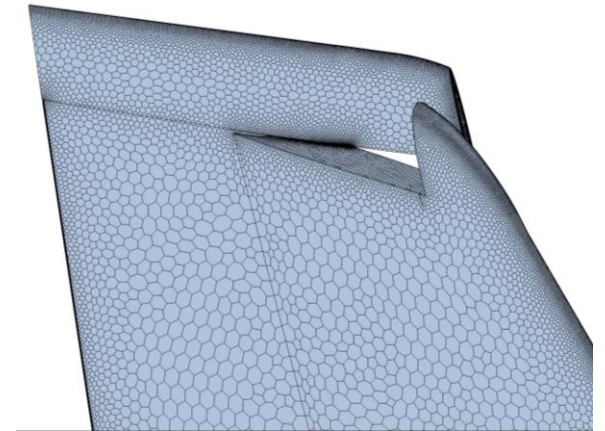
flap deflection



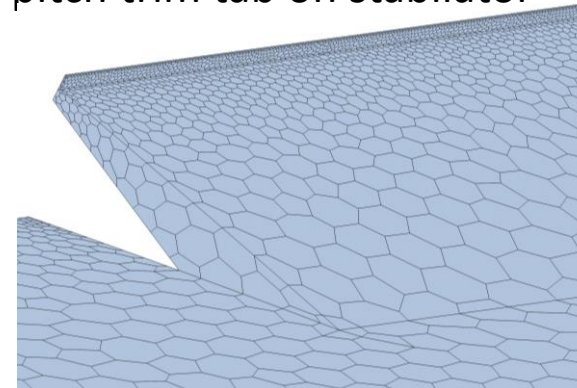
high lift nacelle



rudder deflection



pitch trim tab on stabilator



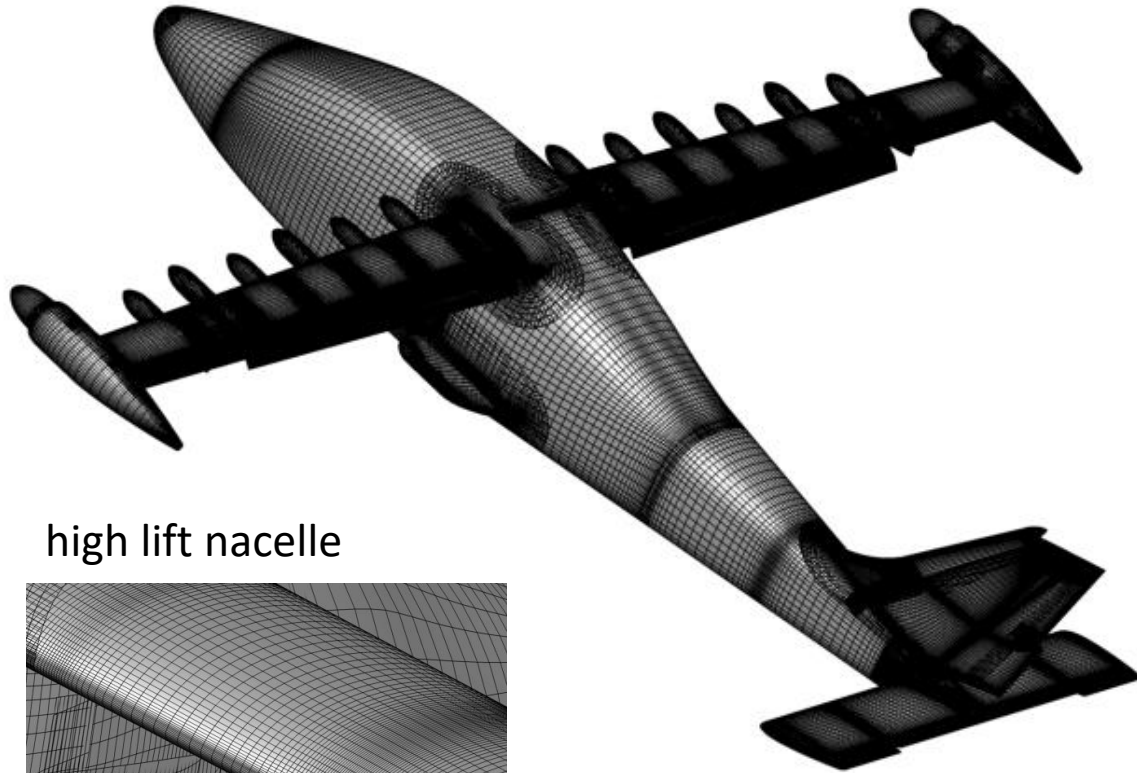
stabilator



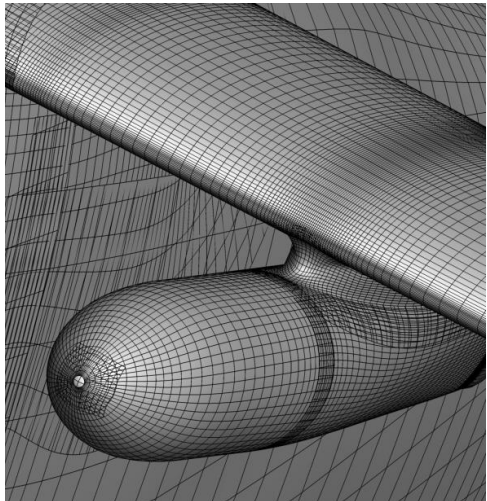


Result – Grid Refinement Study

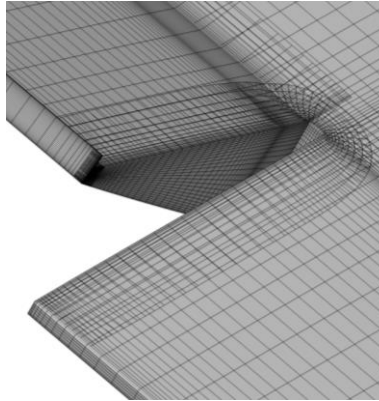
- LAVA structured overset curvilinear grid (coarse grid shown for clarity)



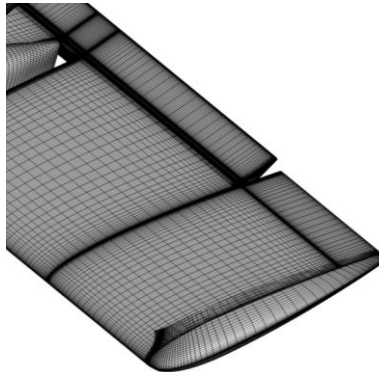
high lift nacelle



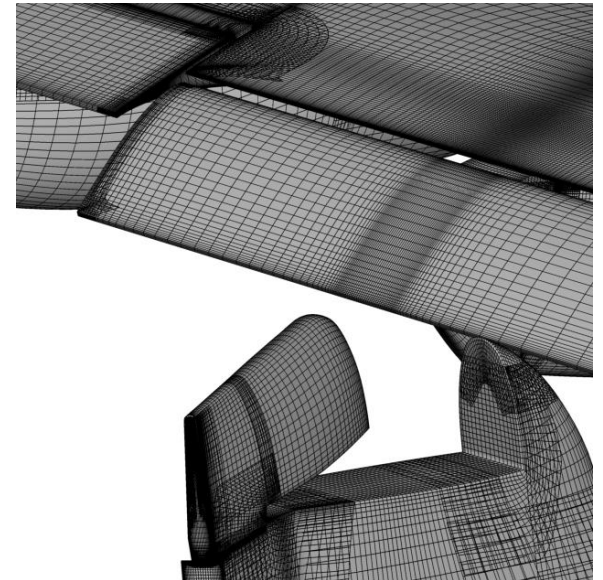
pitch trim tab on stabilator



stabilator



flap and rudder deflection





Result – Grid Refinement Study

- STAR-CCM+
 - 3 resolutions: 45e6 Cells (coarse), 77e6 Cells (medium), 126e6 Cells (fine)
- LAVA
 - 5 resolutions: 60.1e6 nodes (coarse), 95.2e6 nodes (medium), 248.6e6 nodes (fine), 312.6e6 nodes (very-fine), 425.7e6 nodes (extra-fine)



Result – Grid Refinement Study

STAR-CCM+ grid resolution	C_D	C_L	C_Y	C_I	C_m	C_n
coarse (45e6 cells)	0.30394	1.46749	-0.61327	0.01631	2.41895	0.12050
medium (77e6 cells)	0.30623	1.47778	-0.61585	0.02004	2.41327	0.12257
fine (126e6 cells)	0.30797	1.47193	-0.61886	0.01982	2.38941	0.12337

STAR-CCM+ grid resolution	C_D error, %	C_L error, %	C_Y error, %	C_I error, %	C_m error, %	C_n error, %
coarse (45 mil. cell)	-1.1	-0.3	-0.9	-17.7	1.2	-2.3
medium (77 mil. cell)	-0.5	0.4	-0.5	1.1	1.0	-0.6

Although relative error C_I is large, the values are small and coarse mesh chosen to accommodate the large number of runs for limited computing resource



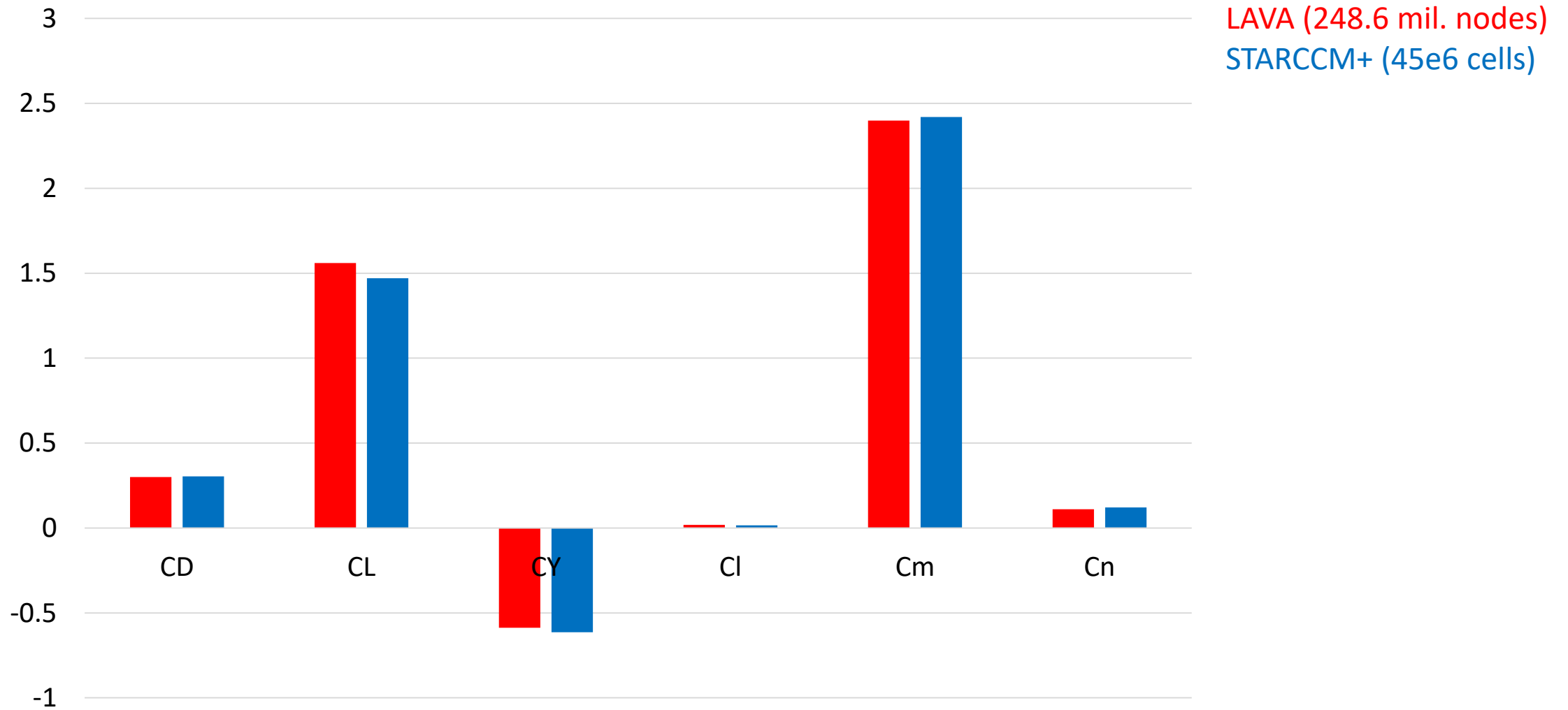
Result – Grid Refinement Study

LAVA grid resolution	C_D	C_L	C_Y	C_I	C_m	C_n
coarse (60.1 mil. nodes)	0.3024	1.57	-0.6053	0.0135	2.396	0.1119
medium (95.2 mil. nodes)	0.29838	1.55	-0.595	0.016	2.404	0.1117
fine (248.6 mil. nodes)	0.30036	1.56	-0.5876	0.0181	2.398	0.1106
very-fine (312.6 mil. nodes)	0.30265	1.56	-0.5844	0.0226	2.402	0.1121
extra-fine (425.7 mil nodes)	0.30237	1.56	-0.582	0.0239	2.401	0.1126

LAVA grid resolution	C_D error, %	C_L error, %	C_Y error, %	C_I error, %	C_m error, %	C_n error, %
coarse (60.1 mil. nodes)	-0.01	-0.64	-4.00	43.51	0.21	0.62
medium (95.2 mil. nodes)	1.32	0.51	-2.23	33.05	-0.12	0.80
fine (248.6 mil. nodes)	0.66	-0.26	-0.96	24.27	0.12	1.78
very-fine (312.6 mil. nodes)	-0.09	-0.32	-0.41	5.44	-0.04	0.44



Result – Grid Refinement Study





Result

- Grid Refinement Study
- Angle of attack sweep
- Sideslip angle sweep



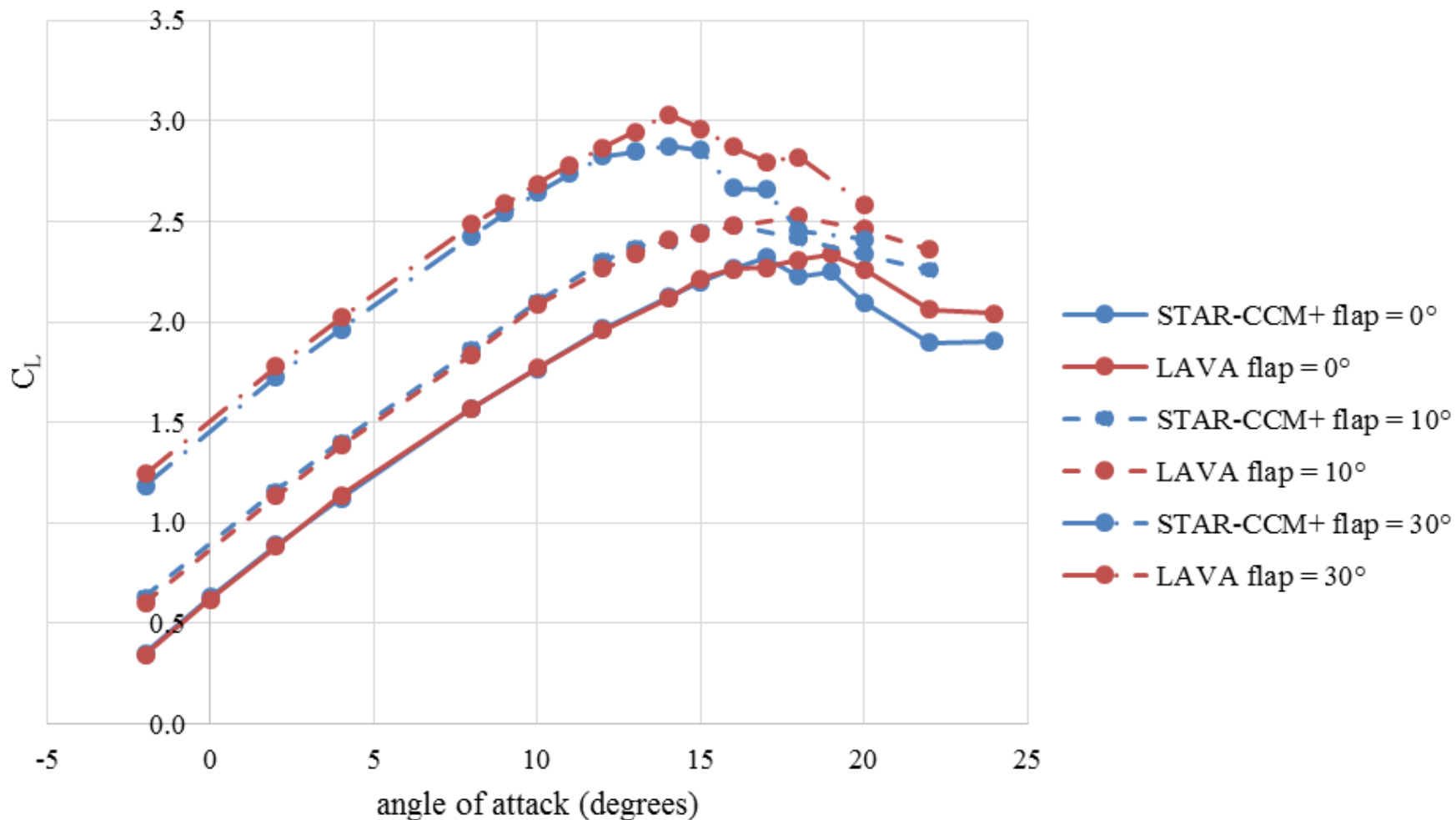
Result – Angle of attack sweep

- 3 flap settings – 0° (cruise) , 10° (take-off), 30° (landing)
- Control surfaces in neutral position (no deflection)

	Flap = 0°	Flap = 10°	Flap = 30°
Altitude, ft	8000	2500	2500
Mach	0.233	0.149	0.139
Density, slug/ft ³	1.8628E-3	2.20782E-3	2.20782E-3
Static pressure, lbf/ft ²	1571.9	1931.9	1931.9
Static temperature, K	272.3	283.2	283.2
Coefficient of viscosity, slug/ft/s	3.57532E-7	3.68708E-7	3.68708E-7
Reynolds number	1.32E6	9.875E5	9.21E5



Result – Angle of attack sweep

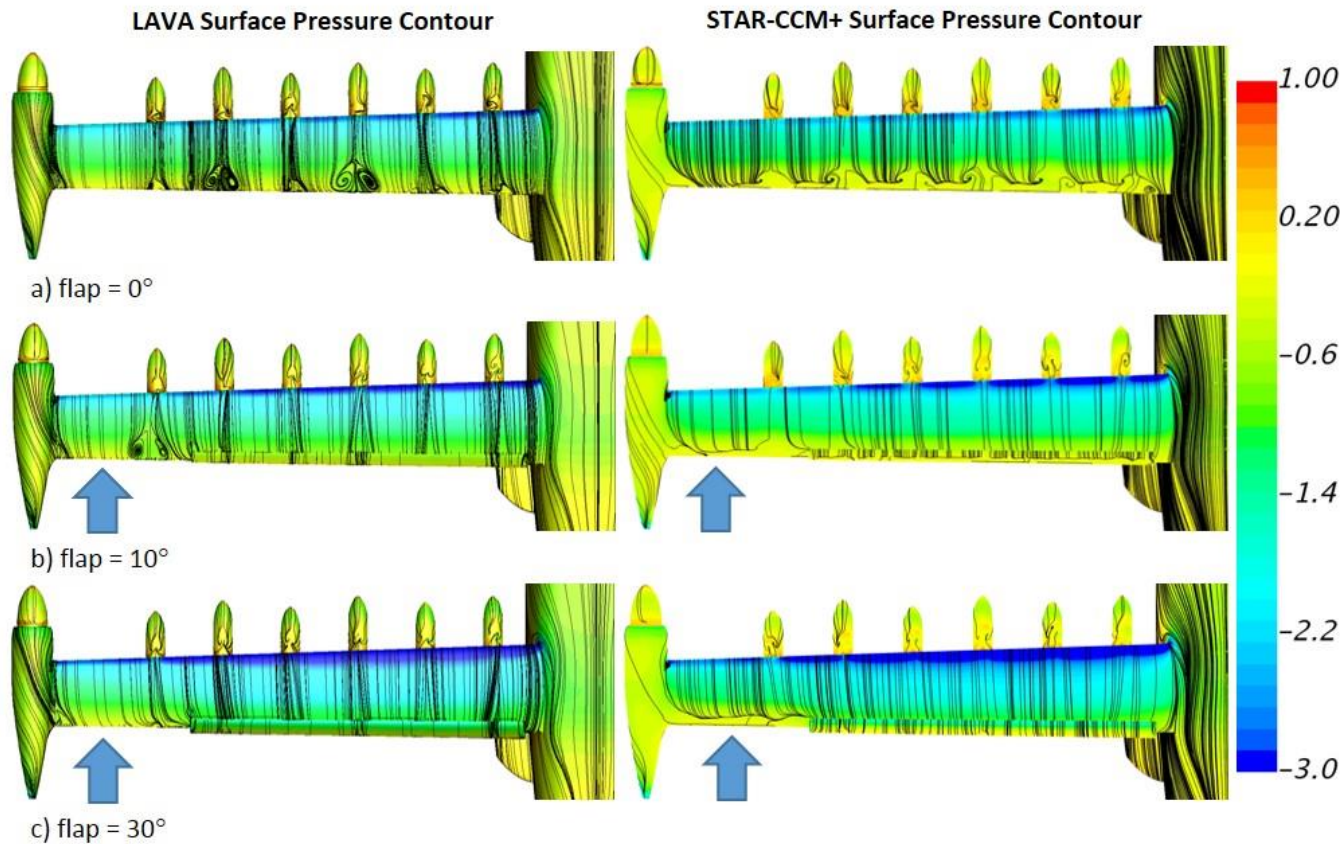


- Lift dependency on flap deflection
 - lift increases with increase in flap deflection angle
 - Angle of attack for maximum lift decreases with increase in flap deflection
- Differences in solver
 - lift at high angle of attack
 - Increase in discrepancy with increase in flap deflection angle at linear region



Result – Angle of attack sweep

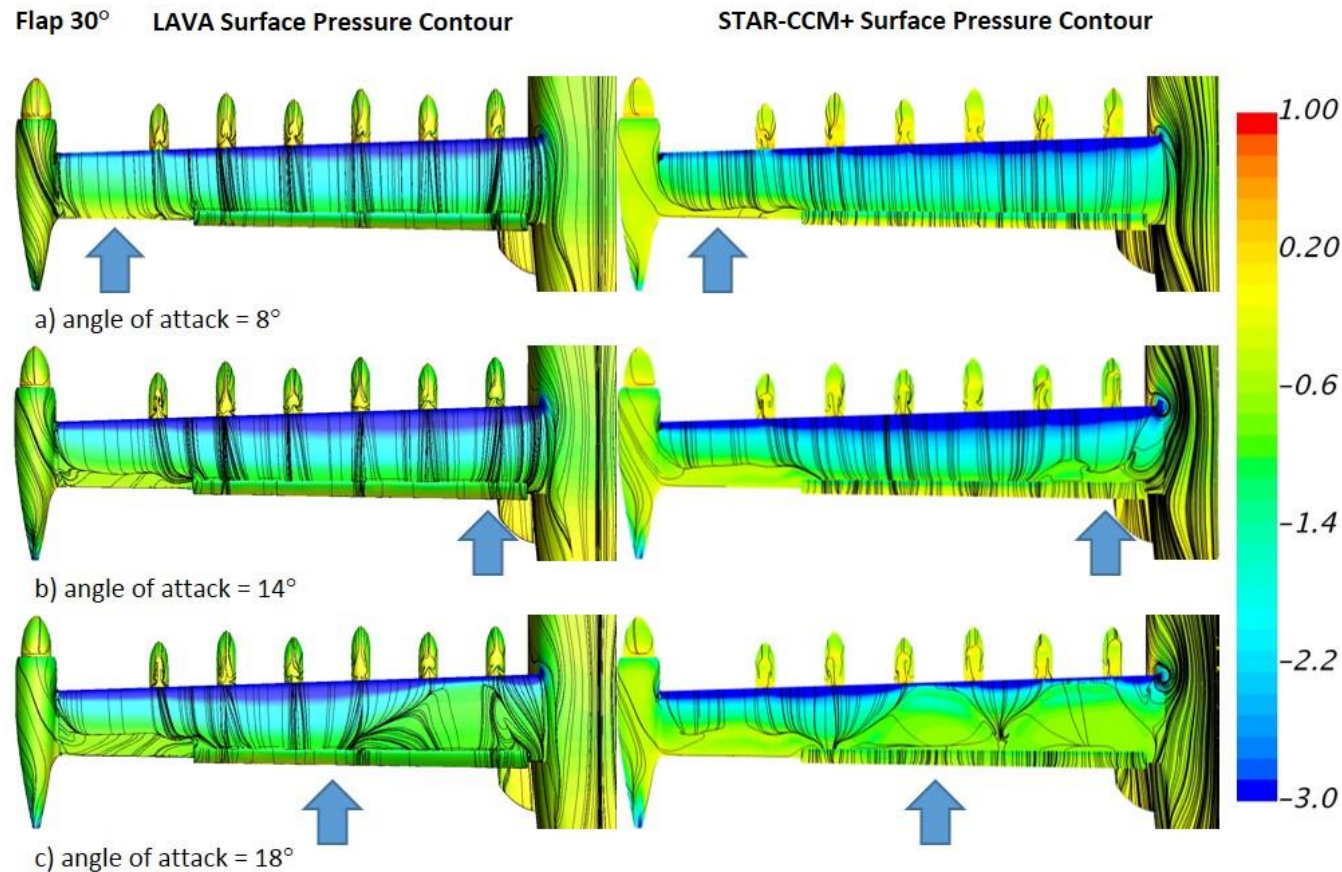
Angle of attack = 8°



- Increase in solution discrepancy in lift with increase in flap deflection angle at linear region
- STAR-CCM+ solution show flow separation at outboard wing that is not show in LAVA for 10° and 30° flap deflection



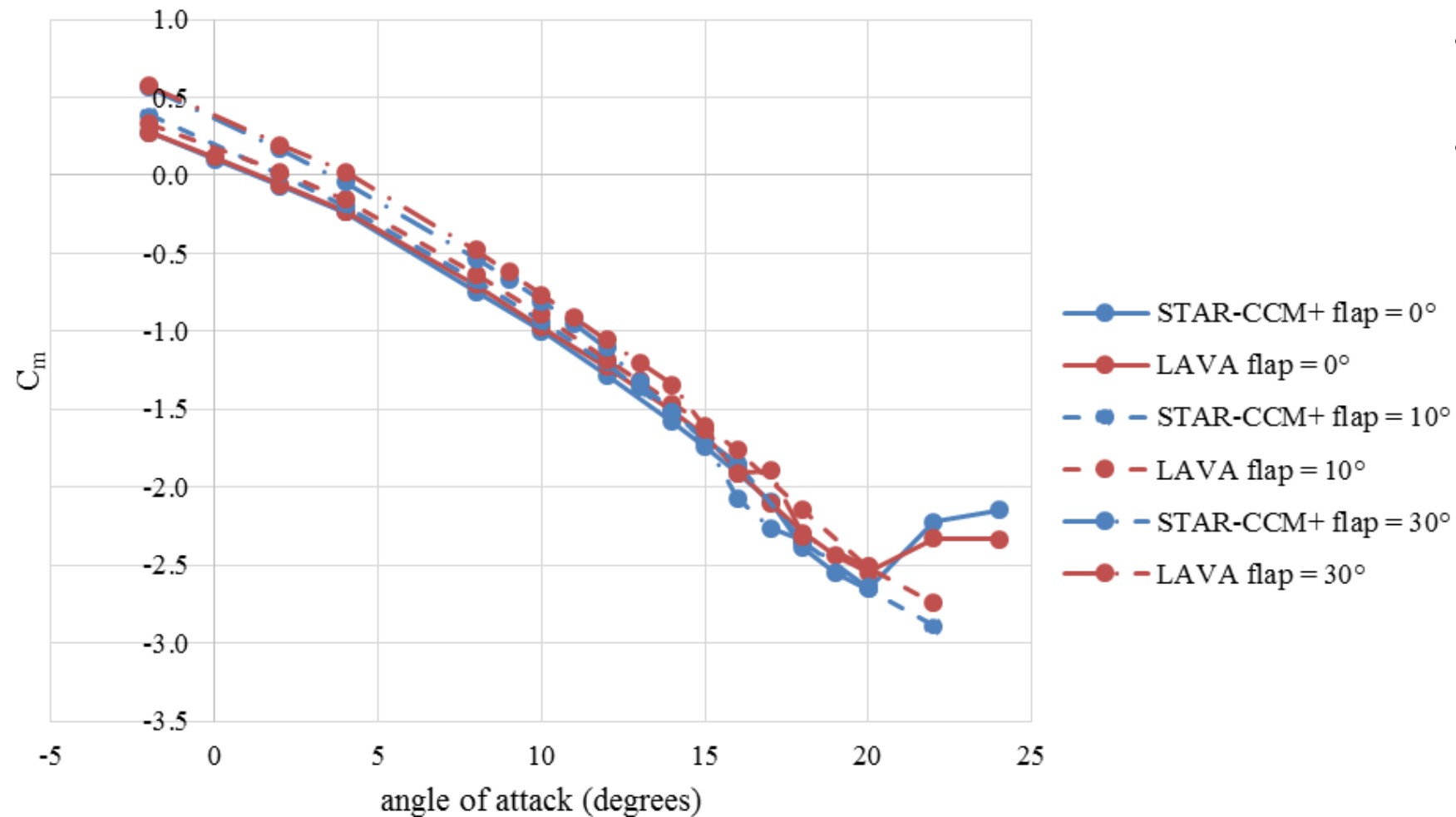
Result – Angle of attack sweep



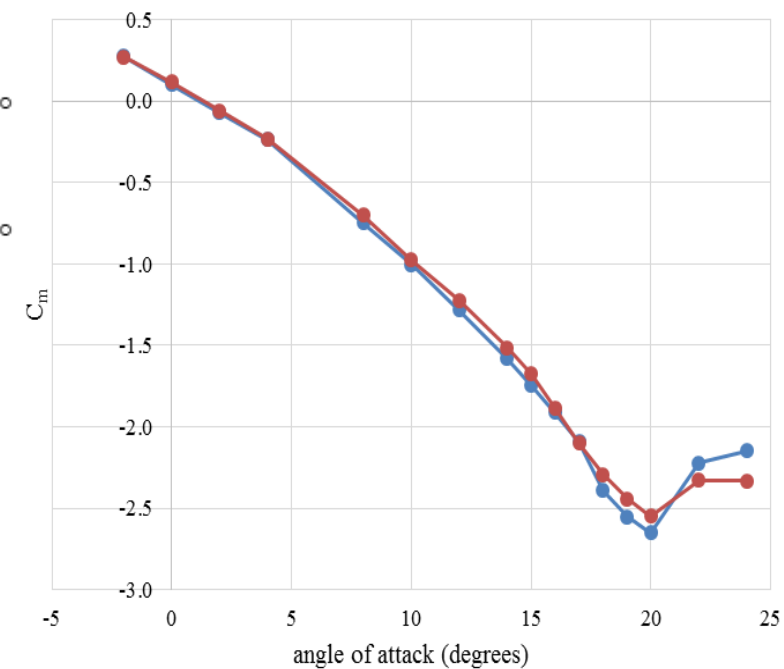
- Increase in solution discrepancy in lift at high angle of attack
- STAR-CCM+ solution show larger region of separated flow at higher angle of attack compared to LAVA



Result – Angle of attack sweep



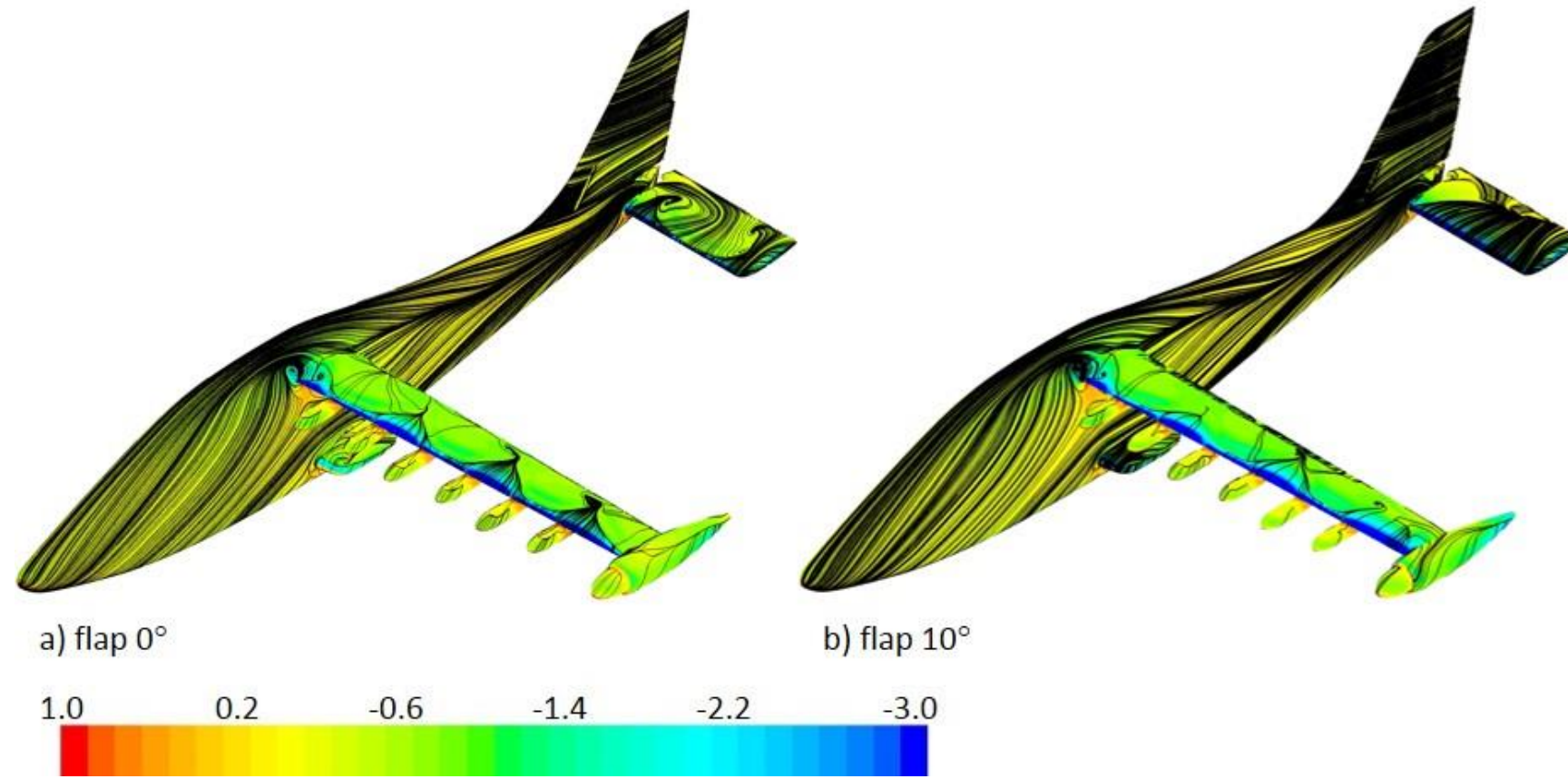
- Higher pitching moment with higher flap deflection angle
- Sharp increase in pitching moment for 0° flap angle at 20° angle of attack





Result – Angle of attack sweep

Angle of attack = 22° , surface pressure contour



- Large flow separation shown on the upper surface of stabilator for 0° flap deflection configuration
- Flow separation shown on the upper surface of stabilator on 10° flap deflection configuration located to inboard and trailing edge



Result

- Grid Refinement Study
- Angle of attack sweep
- Sideslip angle sweep



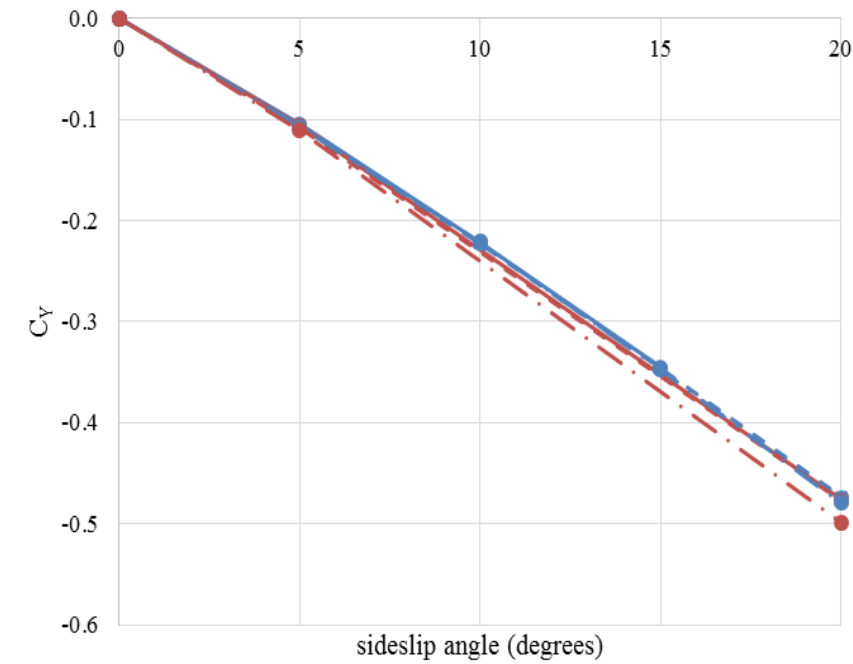
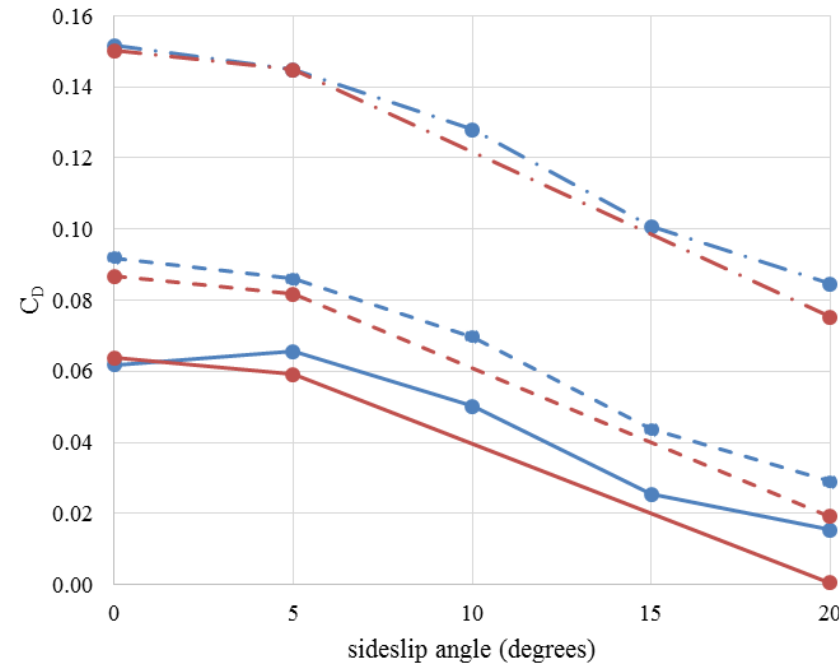
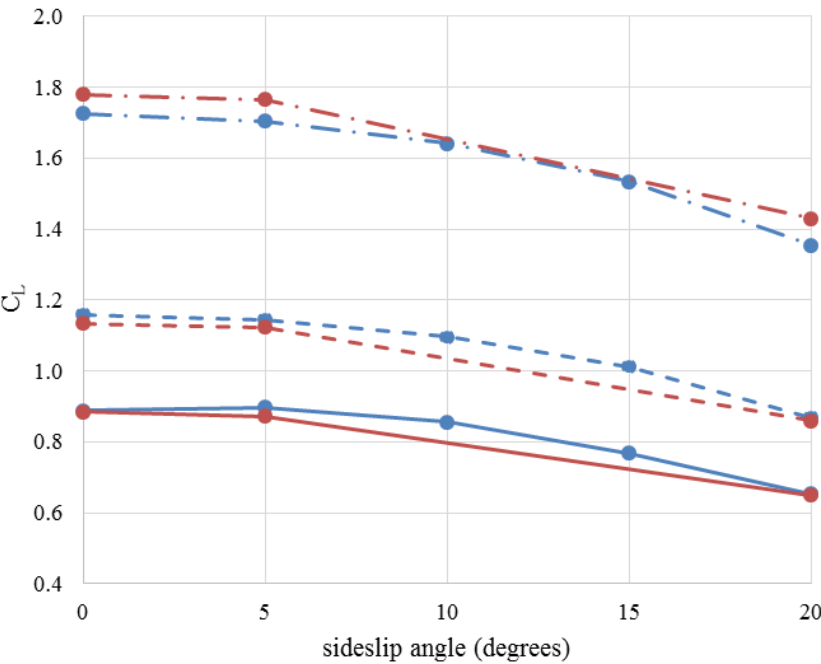
Result – Sideslip angle sweep

- 3 flap settings – 0° (cruise) , 10° (take-off), 30° (landing)
- Control surfaces in neutral position (no deflection)

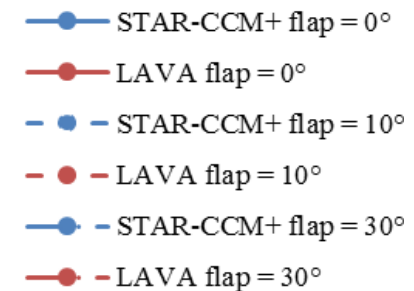
	Flap = 0°	Flap = 10°	Flap = 30°
Altitude, ft	8000	2500	2500
Mach	0.233	0.149	0.139
Density, slug/ft³	1.8628E-3	2.20782E-3	2.20782E-3
Static pressure, lbf/ft²	1571.9	1931.9	1931.9
Static temperature, K	272.3	283.2	283.2
Coefficient of viscosity, slug/ft/s	3.57532E-7	3.68708E-7	3.68708E-7
Reynolds number	1.32E6	9.875E5	9.21E5



Result – Sideslip angle sweep

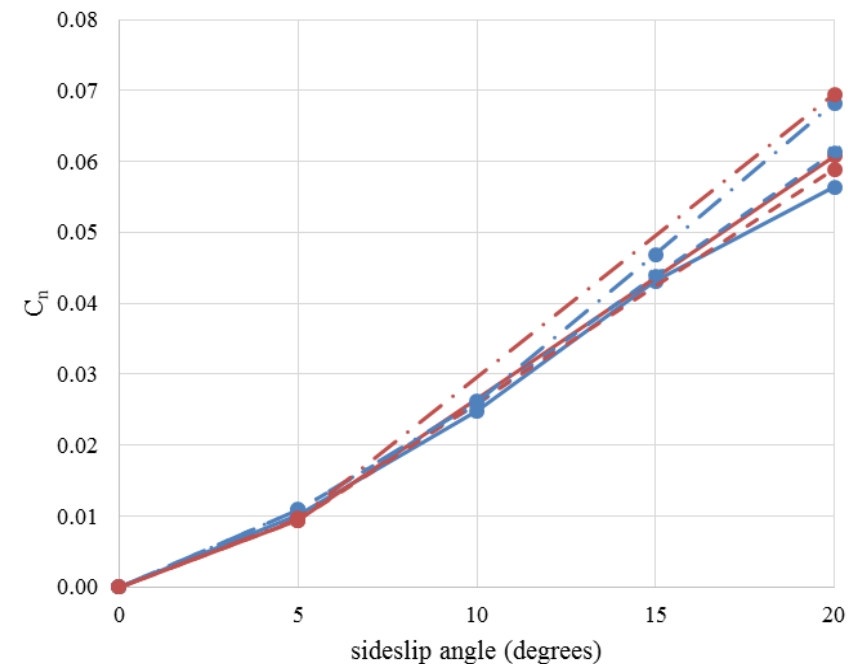
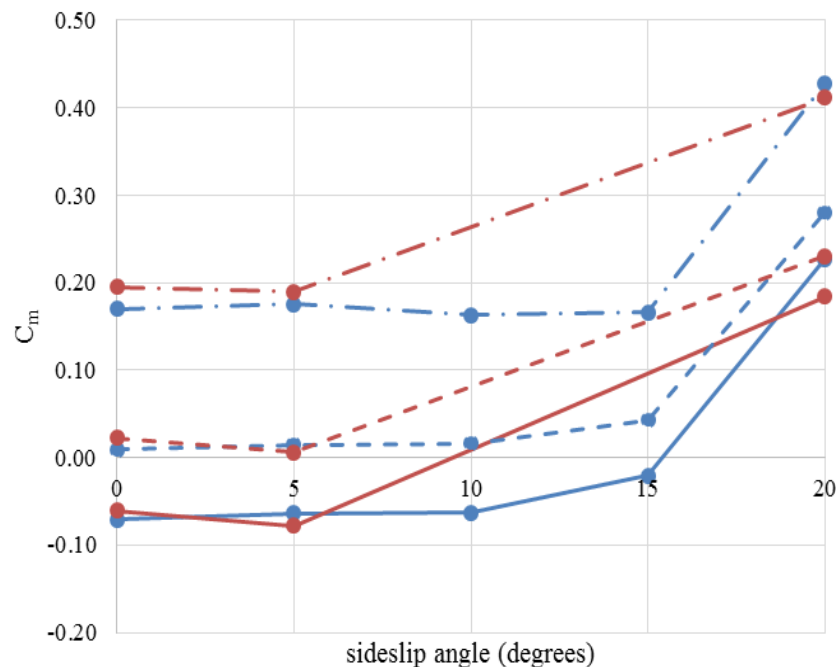
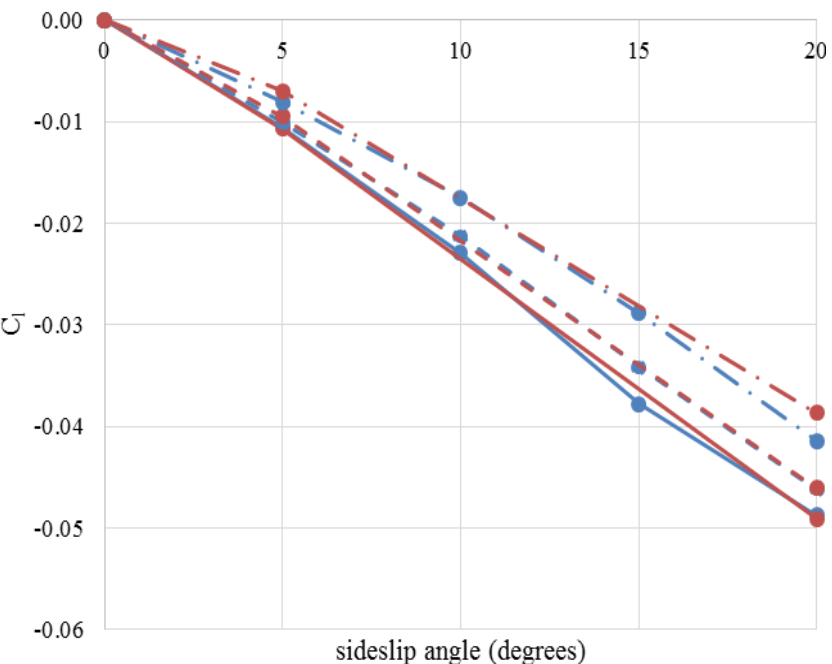


- Lift, drag, side forces all decrease with increasing sideslip angle
- Drag decreasing because it is in stability axis (increases when computed in wind axis)

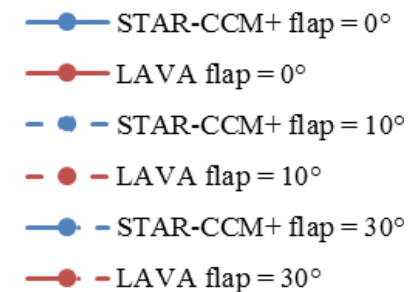




Result – Sideslip angle sweep



- Rolling moment - 30° flap produces least amount of rolling moment
- Pitching moment - sharp increase in at 15° for all flap deflections
- Yawing moment - 30° flap produces least amount of rolling moment





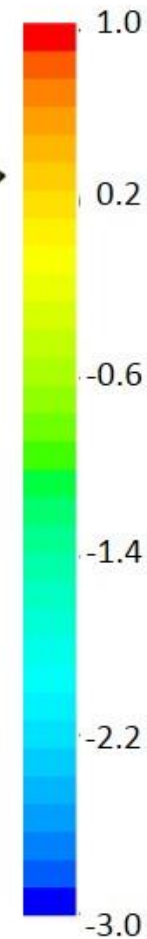
Result – Sideslip angle sweep

surface pressure coefficient, Angle of attack = 22°

a) flap = 0°

b) flap = 10°

c) flap = 30°



- Increasing separation at leading edge of right wing root with increasing flap deflection
- Separated region at the leading edge of rudder



Conclusion

- Unpowered X-57 MOD-III configuration analyzed
- Angle of attack sweep and sideslip angle sweep presented
- STAR-CCM+ and LAVA solution comparison
 - flow visualization show that solution compare well at low angle of attack
 - Difference in predicted separation behavior at higher angle of attack



QUESTION?